

Mass Detection with Nonlinear Nanomechanical Resonator

Eyal Buks

Department of Electrical Engineering, Technion, Haifa 32000 Israel

Bernard Yurke

Bell Laboratories, Lucent Technologies, 600 Mountain Avenue, Murray Hill, NJ 07974

(Dated: April 1, 2022)

Nanomechanical resonators having small mass, high resonance frequency and low damping rate are widely employed as mass detectors. We study the performances of such a detector when the resonator is driven into a region of nonlinear oscillations. We predict theoretically that in this region the system acts as a phase-sensitive mechanical amplifier. This behavior can be exploited to achieve noise squeezing in the output signal when homodyne detection is employed for readout. We show that mass sensitivity of the device in this region may exceed the upper bound imposed by thermomechanical noise upon the sensitivity when operating in the linear region. On the other hand, we show that the high mass sensitivity is accompanied by a slowing down of the response of the system to a change in the mass.

PACS numbers: 42.50.Dv, 05.45.-a

I. INTRODUCTION

Nano-electro-mechanical systems (NEMS) serve in a variety of applications as sensors and actuators. Recent studies have demonstrated ultra-sensitive mass sensors based on NEMS [1, 2, 3, 4, 5, 6, 7, 8, 9, 10, 11, 12, 13]. Such sensors promise a broad range of applications, from ultra-sensitive mass spectrometers that can be used to detect hazardous molecules, through biological applications at the level of a single DNA base-pair, to the study of fundamental questions such as the interaction of a single pair of molecules. In these devices mass detection is achieved by monitoring the resonance frequency ω_0 of one of the modes of a nanomechanical resonator. The dependence of ω_0 on the effective mass m allows for sensitive detection of additional mass being adsorbed on the surfaces of the resonator. In such mass detectors the adsorbent molecules are anchored to the resonator surface either by Van der-Waals interaction, or by covalent bonds to linker molecules that are attached to the surface. Various analytes were used in those experiments, including alcohol and explosive gases, biomolecules, single cells, DNA molecules, and alkane chains. Currently, the smallest detectable mass change is $\delta m \simeq 0.4 \times 10^{-21}$ kg [9], achieved by using a $4 \mu\text{m}$ long silicon beam with a resonance frequency $\omega_0/2\pi = 10$ MHz, a quality factor Q of about 2,500, and total mass $m \simeq 5 \times 10^{-16}$ kg. In a recent experiment Ilic *et al.* [10] succeeded to measure a single DNA molecule of about 1,600 base pairs, which corresponds to $\delta m \simeq 1.6 \times 10^{-21}$ kg, by using a silicon nitride cantilever, and employing an optical detection scheme.

In general, any detection scheme employed for monitoring the mass can be characterized by two important figures of merit. The first is the minimum detectable change in mass δm . This parameter is determined by the responsivity, which is defined as the derivative of the average output signal $\langle X(t) \rangle$ of the detector with respect

to the mass m , the noise level, which is usually characterized by the spectral density of $X(t)$, and by the averaging time τ employed for measuring the output signal $X(t)$. The second figure of merit is the ring-down time t_{RD} , which is a measure of the time width of the step in $X(t)$ due to a sudden change in m .

A number of factors affect the minimum detectable mass δm and the ring-down time t_{RD} of mass detectors, based on nanomechanical resonators. Recent studies [14, 15] have shown that if measurement noise is dominated by thermomechanical fluctuations the following hold

$$\frac{\delta m}{m} = 2 \left(\frac{2\pi}{Q\omega_0\tau} \frac{k_B T}{U_0} \right)^{1/2}, \quad (1)$$

where $k_B T$ is the thermal energy, U_0 is the energy stored in the resonator, and τ is the measurement averaging time, and the ring-down time is given by

$$t_{\text{RD}} = \frac{Q}{\omega_0}. \quad (2)$$

Eq. (1) indicates that nanomechanical resonators having small m and high ω_0 may allow high mass sensitivity (small δm). Further enhancement in the sensitivity can be achieved by increasing Q however, this will be accompanied by an undesirable increase in the ring-down time, namely, slowing down the response of the system to changes in m . Moreover, Eq. (1) apparently suggests that unlimited reduction in δm can be achieved by increasing U_0 by means of increasing the drive amplitude. Note however that Eq. (1), which was derived by assuming the case of linear response, is not applicable in the nonlinear region. Thus, in order to characterize the performances of the system when nonlinear oscillations are excited by an intense drive, one has to generalize the analysis by taking nonlinearity into account. From a

more general point of view, such a generalization is interesting because it provides some insight onto the question of what is the range of applicability of the fluctuation-dissipation theorem for nonlinear systems [16].

In the present paper we generalize Eqs. (1) and (2) and extend their range of applicability by taking into account nonlinearity in the response of the resonator to lowest order. Practically, characterizing the performances of nanomechanical mass detectors in the nonlinear region is important since in many cases, when a displacement detector with a sufficiently high sensitivity is not available, the oscillations of the system in the linear regime cannot be monitored, and consequently operation is possible only in the region of nonlinear oscillations. Another possibility for exploiting nonlinearity for enhancing mass sensitivity was recently studied theoretically by Cleland [15], who has considered the case where the mechanical resonator is excited parametrically.

When nonlinearity is taken into account to lowest order the resonator's dynamics can be described by the Duffing equation of motion [17]. A Duffing resonator may exhibit bistability when driven by an external periodic force with amplitude p exceeding some critical value p_c . Figure 1 below shows the calculated response vs. drive frequency ω_p of a Duffing resonator excited by a driving force with (b) sub-critical $p = p_c/2$ (c) critical $p = p_c$, and (d) over-critical $p = 2p_c$ amplitude. The range of bistability in the (ω_p, p) plane is seen in Fig. 1 (a). As was shown in Ref. [18], high responsivity can be achieved when driving the resonator close to the edge of the bistability region [19, 20, 21, 22, 23], where the slope of the response vs. frequency curve approaches infinity. Note however that in the same region of operation an undesirable slowing down occurs, namely t_{RD} can become much longer than its value in the linear region, which is given by Eq. (2).

The detector's performances depend in general on the detection scheme which is being employed. Here we consider the case of a homodyne detection scheme [18], where the output signal of a displacement detector monitoring the mechanical motion of the resonator is mixed with a local oscillator at the frequency of the driving force and with an adjustable phase ϕ_{LO} . In the nonlinear regime of operation the device acts as a phase sensitive intermodulation amplifier [24]. Consequently, noise squeezing occurs in this regime, as was recently demonstrated experimentally in Ref. [25], namely, the spectral density of the output signal at the IF port of the mixer depends on ϕ_{LO} periodically [26].

To optimize the operation of the system in the nonlinear region it is important to understand the role played by damping. In this region, in addition to linear damping, also nonlinear damping may affect the device performances. Our theoretical analysis [18] shows that instability in a Duffing resonator is accessible only when the nonlinear damping is sufficiently small. Moreover, a fit between theory and experimental results allows extracting the nonlinear damping rate. By employing such a fit it was found in Ref. [27] that nonlinear damping can

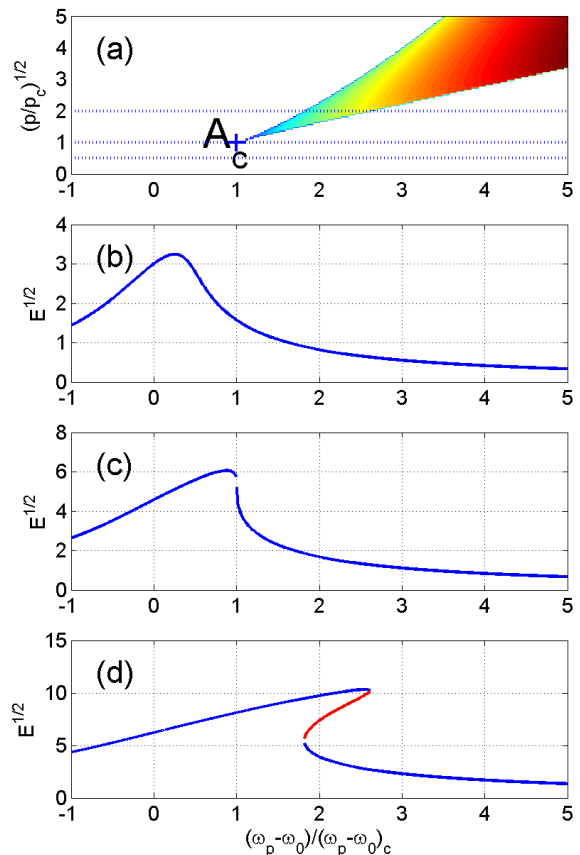


FIG. 1: (Color online) Response of a driven Duffing resonator. Panel (a) shows the bistable region in the (ω_p, p) plane. The response vs. frequency is shown in panel (b), (c) and (d) for sub-critical, critical, and over-critical driving force respectively.

play a significant role in the dynamics in the nonlinear region, and thus we take it into account in our analysis.

The paper is organized as follows. In section II the Hamiltonian of the driven Duffing resonator is introduced. The equations of motion of the system are derived in section III and linearized in section IV. The basins of attraction of the system are presented in section V. The ring-down time is estimated in section VI, whereas the case of homodyne detection is discussed in section VII. The calculation of the spectral density of the output signal of the homodyne detector, which is presented in section VIII, allows to calculate the minimum detectable mass in section IX. We conclude by comparing our findings with the linear case in section X.

II. HAMILTONIAN

Consider a nonlinear mechanical resonator of mass m , resonance frequency ω_0 , damping rate γ , nonlinear Kerr

constant K , and nonlinear damping rate γ_3 . The resonator is driven by harmonic force at frequency ω_p . The complex amplitude of the force f is written as

$$f = -2im\omega_p x_0 p^{1/2} e^{i\phi_p}, \quad (3)$$

where p is positive real, ϕ_p is real, and x_0 is give by

$$x_0 = \sqrt{\frac{\hbar}{2m\omega_0}}. \quad (4)$$

The Hamiltonian of the system is given by [18]

$$H = H_1 + H_{a_2} + H_{a_3} + H_{c_2} + H_{c_3}, \quad (5)$$

where H_1 is the Hamiltonian for the driven nonlinear resonator

$$\begin{aligned} H_1 = & \hbar\omega_0 A^\dagger A + \frac{\hbar}{2} K A^\dagger A^\dagger A A \\ & + \hbar p^{1/2} \left(i e^{i(\phi_p - \omega_p t)} A^\dagger - i e^{-i(\phi_p - \omega_p t)} A \right). \end{aligned} \quad (6)$$

The resonator's creation and annihilation operators satisfy the following commutation relation

$$[A, A^\dagger] = A A^\dagger - A^\dagger A = 1. \quad (7)$$

The Hamiltonians H_{a_2} and H_{a_3} associated with both baths are given by

$$H_{a_2} = \int d\omega \hbar \omega a_2^\dagger(\omega) a_2(\omega), \quad (8)$$

$$H_{a_3} = \int d\omega \hbar \omega a_3^\dagger(\omega) a_3(\omega). \quad (9)$$

The Hamiltonian H_{c_2} linearly couples the bath modes $a_2(\omega)$ to the resonator mode A

$$H_{c_2} = \hbar \sqrt{\frac{\gamma}{\pi}} \int d\omega \left[e^{i\phi_2} A^\dagger a_2(\omega) + e^{-i\phi_2} a_2^\dagger(\omega) A \right], \quad (10)$$

whereas H_{c_3} describes two-phonon absorptive coupling of the resonator mode to the bath modes $a_3(\omega)$ in which two resonator phonons are destroyed for every bath phonon created

$$H_{c_3} = \hbar \sqrt{\frac{\gamma_3}{\pi}} \int d\omega \left[e^{i\phi_3} A^\dagger A^\dagger a_3(\omega) + e^{-i\phi_3} a_3^\dagger(\omega) A A \right]. \quad (11)$$

Both phase factors ϕ_2 and ϕ_3 are real. The bath modes are boson modes, satisfying the usual Bose commutation relations

$$[a_n(\omega), a_n^\dagger(\omega')] = \delta(\omega - \omega'), \quad (12)$$

$$[a_n(\omega), a_n(\omega')] = 0. \quad (13)$$

III. EQUATIONS OF MOTION

We now generate the Heisenberg equations of motion according to

$$i\hbar \frac{dO}{dt} = [O, H], \quad (14)$$

where O is an operator and H is the total Hamiltonian

$$\begin{aligned} i \frac{dA}{dt} = & \omega_0 A + K A^\dagger A A + i p^{1/2} e^{i\phi_p} e^{-i\omega_p t} \\ & + \sqrt{\frac{\gamma}{\pi}} e^{i\phi_2} \int d\omega a_2(\omega) + 2 \sqrt{\frac{\gamma_3}{\pi}} e^{i\phi_3} A^\dagger \int d\omega a_3(\omega), \end{aligned} \quad (15)$$

$$\frac{da_2(\omega)}{dt} = -i\omega a_2(\omega) - i \sqrt{\frac{\gamma}{\pi}} e^{-i\phi_2} A, \quad (16)$$

$$\frac{da_3(\omega)}{dt} = -i\omega a_3(\omega) - i \sqrt{\frac{\gamma_3}{2\pi}} e^{-i\phi_3} A A. \quad (17)$$

Using the standard method of Gardiner and Collett [28], and employing a transformation to a reference frame rotating at angular frequency ω_p

$$A = C e^{-i\omega_p t}, \quad (18)$$

yield the following equation for the operator C

$$\frac{dC}{dt} + \Theta = F(t), \quad (19)$$

where

$$\Theta = [\gamma + i(\omega_0 - \omega_p) + (iK + \gamma_3) C^\dagger C] C - p^{1/2} e^{i\phi_p}. \quad (20)$$

The noise term $F(t)$ is given by

$$F = -i \sqrt{2\gamma} e^{i\phi_2} a_2^{in} e^{i\omega_p t} - i 2 \sqrt{\gamma_3} e^{i\phi_3} C^\dagger a_3^{in} e^{2i\omega_p t}, \quad (21)$$

where

$$a_2^{in}(t) = \frac{1}{\sqrt{2\pi}} \int d\omega e^{-i\omega(t-t_0)} a_2(t_0, \omega), \quad (22)$$

$$a_3^{in}(t) = \frac{1}{\sqrt{2\pi}} \int d\omega e^{-i\omega(t-t_0)} a_3(t_0, \omega). \quad (23)$$

Note that in the noiseless case, namely when $F = 0$, the equation of motion for the displacement x of the vibrating mode can be written as

$$\begin{aligned} \frac{d^2x}{dt^2} + 2\gamma \left[1 + \frac{\gamma_3}{3\gamma} \left(\frac{x}{x_0} \right)^2 \right] \frac{dx}{dt} + \omega_0^2 \left[1 + \frac{2K}{3\omega_0} \left(\frac{x}{x_0} \right)^2 \right] x \\ = \frac{f}{m} e^{-i\omega_p t} + c.c. . \end{aligned} \quad (24)$$

IV. LINEARIZATION

Let $C = C_m + c$, where C_m is a complex number for which

$$\Theta(C_m, C_m^*) = 0 , \quad (25)$$

namely, C_m is a steady state solution of Eq. (19) for the noiseless case $F = 0$. When the noise term F can be considered as small, one can find an equation of motion for the fluctuation around C_m by linearizing Eq. (19)

$$\frac{dc}{dt} + Wc + Vc^\dagger = F , \quad (26)$$

where

$$W = \left. \frac{\partial \Theta}{\partial C} \right|_{C=C_m} = \gamma + i(\omega_0 - \omega_p) + 2(iK + \gamma_3) C_m^* C_m , \quad (27)$$

and

$$V = \left. \frac{\partial \Theta}{\partial C^\dagger} \right|_{C=C_m} = (iK + \gamma_3) C_m^2 . \quad (28)$$

A. Mean-Field Solution

Using the notation

$$C_m = E^{1/2} e^{i\phi_m} , \quad (29)$$

where E is positive and ϕ_m is real, Eq. (25) reads

$$[\gamma + i(\omega_0 - \omega_p) + (iK + \gamma_3) E] E^{1/2} e^{i\phi_m} = p^{1/2} e^{i\phi_p} . \quad (30)$$

Multiplying each side by its complex conjugate yields

$$\left[(\gamma + \gamma_3 E)^2 + (\omega_0 - \omega_p + KE)^2 \right] E = p . \quad (31)$$

Finding E by solving the cubic polynomial Eq. (31) allows calculating C_m using Eq. (30).

Taking the derivative of Eq. (31) with respect to the drive frequency ω_p , one finds

$$\frac{\partial E}{\partial \omega_p} = \frac{2(\omega_0 - \omega_p + KE)E}{|W|^2 (1 - \zeta^2)} , \quad (32)$$

where

$$\zeta = \left| \frac{V}{W} \right| . \quad (33)$$

Similarly for the drive amplitude p

$$\frac{\partial E}{\partial p} = \frac{1}{|W|^2 (1 - \zeta^2)} . \quad (34)$$

Note that, as will be shown below, the value $\zeta = 1$ occurs along the edge of the bistability region.

B. The bifurcation point

At the bifurcation point, namely at the onset of bistability, the following holds

$$\frac{\partial \omega_p}{\partial E} = \frac{\partial^2 \omega_p}{\partial E^2} = 0 . \quad (35)$$

Such a point occurs only if the nonlinear damping is sufficiently small [18], namely, only when the following condition holds

$$|K| > \sqrt{3}\gamma_3 . \quad (36)$$

At the bifurcation point the drive frequency and amplitude are given by

$$(\omega_p - \omega_0)_c = \gamma \frac{K}{|K|} \left[\frac{4\gamma_3 |K| + \sqrt{3}(K^2 + \gamma_3^2)}{K^2 - 3\gamma_3^2} \right] , \quad (37)$$

$$p_c = \frac{8}{3\sqrt{3}} \frac{\gamma^3 (K^2 + \gamma_3^2)}{(|K| - \sqrt{3}\gamma_3)^3} , \quad (38)$$

and the resonator mode amplitude is

$$E_c = \frac{2\gamma}{\sqrt{3}(|K| - \sqrt{3}\gamma_3)} . \quad (39)$$

V. BASINS OF ATTRACTION

In the bistable region Eq. (25) has 3 different solutions, labeled as C_1 , C_2 and C_3 , where both stable solutions C_1 and C_3 are attractors, and the unstable solution C_2 is a saddle point. The bistable region Λ

in the plane of parameters (ω_p, p) is seen in the colormap in Fig. 1 (a). The Kerr constant in this example is $K/\omega_0 = 0.001$, and the damping constants are $\gamma/\omega_0 = 0.02$, $\gamma_3 = 0.1K/\sqrt{3}$. The color in the bistable region Λ indicates the difference $|C_3|^2 - |C_1|^2$. The bifurcation point at $\omega_p - \omega_0 = (\omega_p - \omega_0)_c$ and $p = p_c$ is labeled as A_c in the figure.

Figure 2 (a) shows some flow lines obtained by integrating Eq. (19) numerically for the noiseless case $F = 0$. The red and blue lines represent flow toward the attractors at C_1 and C_3 respectively. The green line is the separatrix, namely the boundary between the basins of attraction of the attractors at C_1 and C_3 . A closer view of the region near C_1 and C_2 is given in Fig. 2 (b). This figure shows also, an example of a random motion near the attractor at C_1 (seen as a cyan line). The line was obtained by numerically integrating Eq. (19) with a non vanishing fluctuating force F . The random walk demonstrates noise squeezing (to be further discussed below), where the fluctuations obtain their largest and smallest values along the directions of the local principle axes (see appendix).

VI. RING-DOWN TIME

The solution of the equation of motion (26) was found in Ref. [18]

$$c(t) = \int_{-\infty}^{\infty} dt' G(t-t') \Gamma(t'), \quad (40)$$

where

$$\Gamma(t) = \frac{dF(t)}{dt} + W^* F(t) - V F^\dagger(t). \quad (41)$$

The propagator is given by

$$G(t) = u(t) \frac{e^{-\lambda_0 t} - e^{\lambda_1 t}}{\lambda_1 - \lambda_0}, \quad (42)$$

where $u(t)$ is the unit step function

$$u(t) = \begin{cases} 1, & t > 0 \\ 1/2, & t = 0 \\ 0, & t < 0 \end{cases}, \quad (43)$$

and λ_0 and λ_1 are the eigenvalues of the homogeneous equation, which satisfy

$$\lambda_0 + \lambda_1 = 2W', \quad (44)$$

$$\lambda_0 \lambda_1 = |W|^2 - |V|^2, \quad (45)$$

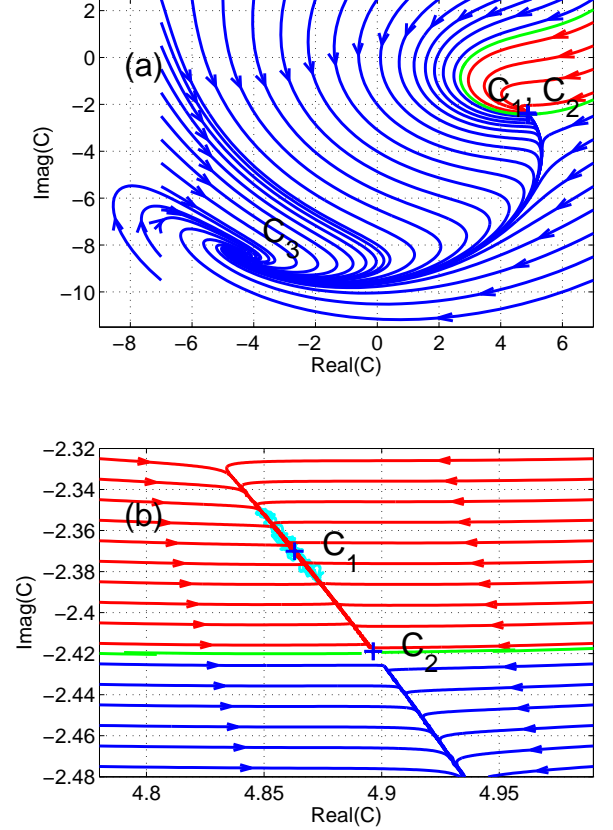


FIG. 2: (Color online) Flow lines obtained by integrating Eq. (19) for the noiseless case $F = 0$. The points C_1 and C_3 are attractors, and C_2 is a saddle point. The green line is the separatrix, namely the boundary between the basins of attraction of both attractors. Panel (a) shows a wide view, whereas panel (b) shows a closer view of the region near C_1 and C_2 . The cyan line near the attractor C_1 in panel (b) demonstrates random motion in the presence of noise.

where W' is the real part of W . Thus one has

$$\lambda_{0,1} = W' \left(1 \pm \sqrt{1 + \frac{|W|^2}{(W')^2} (\zeta^2 - 1)} \right), \quad (46)$$

or

$$\lambda_{0,1} = \gamma + 2\gamma_3 E \pm \sqrt{(K^2 + \gamma_3^2) E^2 - (\omega_0 - \omega_p + 2KE)^2}. \quad (47)$$

We chose to characterize the ring-down time scale as

$$t_{\text{RD}} = (\lambda_0 \lambda_1)^{-1/2} = \frac{1}{|W| \sqrt{1 - \zeta^2}}. \quad (48)$$

Note that in the limit $\zeta \rightarrow 1$ slowing down occurs and $t_{\text{RD}} \rightarrow \infty$. This limit corresponds to the case of operating

the resonator near a jump point close to the edge of the bistability region.

VII. HOMODYNE DETECTION

Consider the case where homodyne detection is employed for readout. In this case the output signal of a displacement detector monitoring the mechanical motion is mixed with a local oscillator at the same frequency as the frequency of the pump ω_p and having an adjustable phase ϕ_{LO} (ϕ_{LO} is real). The local oscillator is assumed to be noiseless. The output signal of the homodyne detector is proportional to

$$X_{\phi_{\text{LO}}}(t) = e^{i\phi_{\text{LO}}} C(t) + e^{-i\phi_{\text{LO}}} C^\dagger(t) . \quad (49)$$

For the stationary case of a fixed mass m the time varying signal $X_{\phi_{\text{LO}}}(t)$ can be characterized by its average

$$X_0 = \langle X_{\phi_{\text{LO}}}(t) \rangle , \quad (50)$$

and by its time auto-correlation function

$$K(t' - t) = \langle [X_{\phi_{\text{LO}}}(t) - X_0] [X_{\phi_{\text{LO}}}(t') - X_0] \rangle . \quad (51)$$

The correlation function is expected to be an even function of $t' - t$ with a maximum at $t' - t = 0$. The correlation time characterizes the width of that peak. Consider a measurement in which $X_{\phi_{\text{LO}}}(t)$ is continuously monitored in the time interval $[0, \tau]$. Let X_τ be an estimator of the average value of $X_{\phi_{\text{LO}}}(t)$

$$X_\tau = \frac{1}{\tau} \int_0^\tau dt X_{\phi_{\text{LO}}}(t) . \quad (52)$$

Clearly X_τ is unbiased, and its variance is given by

$$\langle (X_\tau - X_0)^2 \rangle = \frac{1}{\tau^2} \int_0^\tau dt \int_0^\tau dt' K(t' - t) . \quad (53)$$

Assuming the case where the measurement time τ is much longer than the correlation time. For this case one can employ the approximation

$$\langle (X_\tau - X_0)^2 \rangle = \frac{1}{\tau} \int_{-\infty}^\infty dt K(t) , \quad (54)$$

or in terms of the spectral density $P_{\phi_{\text{LO}}}(\omega)$ of $X_{\phi_{\text{LO}}}(t)$

$$\langle (X_\tau - X_0)^2 \rangle = \frac{2\pi}{\tau} P_{\phi_{\text{LO}}}(0) . \quad (55)$$

The responsivity R of the detection scheme is defined as

$$R = \left| \frac{\partial X_0}{\partial m} \right| . \quad (56)$$

Using Eq. (55) one finds that the minimum detectable change in mass is given by

$$\delta m = R^{-1} \left(\frac{2\pi}{\tau} \right)^{1/2} P_{\phi_{\text{LO}}}^{1/2}(0) . \quad (57)$$

Moreover, since ω_0 is expected to be proportional to $m^{-1/2}$ one has

$$\frac{\delta m}{m} = \frac{2}{\omega_0} \left(\frac{2\pi}{\tau} \right)^{1/2} \left| \frac{\partial X_0}{\partial \omega_0} \right|^{-1} P_{\phi_{\text{LO}}}^{1/2}(0) . \quad (58)$$

VIII. SPECTRAL DENSITY

To calculate the spectral density $P_{\phi_{\text{LO}}}(\omega)$ of $X_{\phi_{\text{LO}}}(t)$ it is convenient to introduce the Fourier transform

$$c(t) = \frac{1}{\sqrt{2\pi}} \int_{-\infty}^\infty d\omega c(\omega) e^{-i\omega t} , \quad (59)$$

$$\Gamma(t) = \frac{1}{\sqrt{2\pi}} \int_{-\infty}^\infty d\omega \Gamma(\omega) e^{-i\omega t} . \quad (60)$$

Assuming the bath modes are in thermal equilibrium, one finds

$$\langle F(\tau) \rangle = \langle F^\dagger(\tau) \rangle = 0 , \quad (61)$$

$$\langle F(\tau) F(\tau') \rangle = \langle F^\dagger(\tau) F^\dagger(\tau') \rangle = 0 , \quad (62)$$

$$\langle F(\tau) F^\dagger(\tau') \rangle = (\lambda_0 + \lambda_1) \delta(\tau - \tau') \langle n_{\omega_0} \rangle , \quad (63)$$

$$\langle F^\dagger(\tau) F(\tau') \rangle = (\lambda_0 + \lambda_1) \delta(\tau - \tau') (\langle n_{\omega_0} \rangle + 1) . \quad (64)$$

where

$$\langle n_\omega \rangle = \frac{1}{e^{\beta \hbar \omega} - 1} , \quad (65)$$

and $\beta = 1/k_B T$.

In Ref. [18, 29] we have found that the following holds

$$c(\omega) = \frac{\Gamma(\omega)}{(-i\omega + \lambda_0)(-i\omega + \lambda_1)} . \quad (66)$$

where

$$\langle \Gamma(\omega) \rangle = \langle \Gamma^\dagger(\omega) \rangle = 0, \quad (67)$$

$$\langle \Gamma(\omega') \Gamma(\omega) \rangle = \mathcal{N}_1(\omega) \delta(\omega + \omega'), \quad (68)$$

$$\langle \Gamma^\dagger(\omega') \Gamma^\dagger(\omega) \rangle = \mathcal{N}_1^*(\omega) \delta(\omega + \omega'), \quad (69)$$

$$\langle \Gamma^\dagger(\omega') \Gamma(\omega) \rangle + \langle \Gamma(\omega') \Gamma^\dagger(\omega) \rangle = \mathcal{N}_2(\omega) \delta(\omega - \omega'), \quad (70)$$

and

$$\mathcal{N}_1(\omega) = 2W'W^*V \coth \frac{\beta\hbar\omega_0}{2}, \quad (71)$$

$$\mathcal{N}_2 = 2W' \left(|W + i\omega|^2 + |V|^2 \right) \coth \frac{\beta\hbar\omega_0}{2}. \quad (72)$$

The frequency auto-correlation function of $X_{\phi_{\text{LO}}}$ is related to the spectral density $P_{\phi_{\text{LO}}}(\omega)$ by

$$\langle X_{\phi_{\text{LO}}}(\omega') X_{\phi_{\text{LO}}}(\omega) \rangle = P_{\phi_{\text{LO}}}(\omega) \delta(\omega - \omega'), \quad (73)$$

thus one finds

$$\begin{aligned} P_{\phi_{\text{LO}}}(\omega) &= \frac{e^{2i\phi_{\text{LO}}} \mathcal{N}_1(\omega)}{(i\omega + \lambda_0)(i\omega + \lambda_1)(-i\omega + \lambda_0)(-i\omega + \lambda_1)} \\ &+ \frac{e^{-2i\phi_{\text{LO}}} \mathcal{N}_1^*(\omega)}{(-i\omega + \lambda_0^*)(-i\omega + \lambda_1^*)(i\omega + \lambda_0^*)(i\omega + \lambda_1^*)} \\ &+ \frac{\mathcal{N}_2(\omega)}{(i\omega + \lambda_0^*)(i\omega + \lambda_1^*)(-i\omega + \lambda_0)(-i\omega + \lambda_1)}, \end{aligned} \quad (74)$$

or in terms of the factors W and V

$$\begin{aligned} P_{\phi_{\text{LO}}}(\omega) &= \frac{e^{2i\phi_{\text{LO}}} W^*V + e^{-2i\phi_{\text{LO}}} WV^* + |W + i\omega|^2 + |V|^2}{(\omega - i\lambda_0)(\omega + i\lambda_0)(\omega - i\lambda_1)(\omega + i\lambda_1)} \\ &\times 2W' \coth \frac{\beta\hbar\omega}{2}. \end{aligned} \quad (75)$$

1. Spectral Density at $\omega = 0$

At frequency $\omega = 0$ one finds

$$P_{\phi_{\text{LO}}}(0) = \frac{1 + 2\zeta \cos(\phi_{\text{LO}} - \phi_0) + \zeta^2}{(1 - \zeta^2)^2} \frac{2W'}{|W|^2} \coth \frac{\beta\hbar\omega_0}{2}, \quad (76)$$

where the phase factor ϕ_0 is defined in Eq. (A7). The largest value

$$[P_\phi(0)]_{\text{max}} = \frac{1}{(1 - \zeta)^2} \frac{2W'}{|W|^2} \coth \frac{\beta\hbar\omega_0}{2}, \quad (77)$$

is obtained when $\cos(\phi_{\text{LO}} - \phi_0) = 1$, and the smallest value

$$[P_\phi(0)]_{\text{min}} = \frac{1}{(1 + \zeta)^2} \frac{2W'}{|W|^2} \coth \frac{\beta\hbar\omega_0}{2}, \quad (78)$$

when $\cos(\phi_{\text{LO}} - \phi_0) = -1$.

2. Integrated Spectral Density

The integral over all frequencies of the spectral density is easily calculated by employing the residue theorem

$$\frac{\int_{-\infty}^{\infty} P_{\phi_{\text{LO}}}(\omega) d\omega}{2\pi W' \coth \frac{\beta\hbar\omega_0}{2}} = \frac{e^{2i\phi_{\text{LO}}} W^*V + e^{-2i\phi_{\text{LO}}} WV^* + 2|W|^2}{\lambda_0\lambda_1(\lambda_0 + \lambda_1)}. \quad (79)$$

Using Eqs. (44) and (45) one finds

$$\frac{1}{2\pi} \int_{-\infty}^{\infty} P_{\phi_{\text{LO}}}(\omega) d\omega = \frac{1 + \zeta \cos(\phi_{\text{LO}} - \phi_0)}{1 - \zeta^2} \coth \frac{\beta\hbar\omega_0}{2}. \quad (80)$$

Thus, the integrated spectral density peaks and deeps simultaneously with $P_{\phi_{\text{LO}}}(0)$.

IX. MINIMUM DETECTABLE MASS

To evaluate δm using Eq. (58) the responsivity factor $\partial X_0 / \partial \omega_0$ has to be determined. Consider a small change $\delta \omega_0$ in the resonance frequency. Let c_m be the resultant change in the steady state amplitude C_m (here c_m is considered as a c-number). Using Eqs. (25), (27), and (28) one finds

$$-iC_m(\delta\omega_0) = Wc_m + Vc_m^*. \quad (81)$$

Employing a coordinate transformation to the local principal axes (see appendix) and using Eq. (A11) one finds

$$|C_m| e^{i\phi_C}(\delta\omega_0) = [(|W| + |V|)\xi + i(|W| - |V|)\eta], \quad (82)$$

where

$$\phi_C = \phi_m - \phi_a - \pi/2, \quad (83)$$

and the phase factor ϕ_m is defined by Eq. (29). The inverse transformation Eq. (A3) and Eq. (A7) yield

$$c_m = e^{-i\phi_0} \left| \frac{C_m}{W} \right| \left(\frac{\cos \phi_C}{1 + \zeta} + \frac{i \sin \phi_C}{1 - \zeta} \right) (\delta\omega_0) , \quad (84)$$

or

$$c_m = e^{-i\phi_0} \left| \frac{C_m}{W} \right| \frac{e^{i\phi_C} - \zeta e^{-i\phi_C}}{1 - \zeta^2} (\delta\omega_0) . \quad (85)$$

The change in X_0 is given by $\delta X_0 = e^{i\phi_{LO}} c_m + e^{-i\phi_{LO}} c_m^*$, thus one has

$$\frac{\partial X_0}{\partial \omega_0} = 2 \left| \frac{C_m}{W} \right| \text{Re} \left(e^{i(\phi_{LO} - \phi_0 + \phi_C)} \frac{1 - \zeta e^{-2i\phi_C}}{1 - \zeta^2} \right) . \quad (86)$$

Finally, using Eqs. (58), (76), and (86), and assuming the case of high temperature

$$\beta \hbar \omega_0 \ll 1 , \quad (87)$$

one finds

$$\frac{\delta m}{m} = 2 \left(\frac{2\pi}{Q_{\text{eff}} \omega_0 \tau} \frac{k_B T}{U_0} \right)^{1/2} g(\phi_{LO} - \phi_0) , \quad (88)$$

where $Q_{\text{eff}} = \omega_0/W'$ is the effective quality factor, the function g is given by

$$g(\phi) = \frac{[1 + 2\zeta \cos \phi + \zeta^2]^{1/2}}{|\cos(\phi + \phi_C) - \zeta \cos(\phi - \phi_C)|} , \quad (89)$$

and

$$U_0 = \hbar \omega_0 |C_m|^2 . \quad (90)$$

In view of a comparison between Eq. (1) and Eq. (88) we refer to the case where $g < 1$ as the case where the lower bound imposed upon the minimum detectable mass of a linear resonator is exceeded. The function $g(\phi_{LO} - \phi_0)$ is plotted in Fig. (3) (a) for the case $\zeta = 0.1$ and $\phi_C = 0.5\pi$, and in Fig. (3) (b) for the case $\zeta = 0.99$ and $\phi_C = 0.5\pi$. For both cases values of g below unity are obtained in some range of ϕ_{LO} . Figure (3) (c) shows the minimum value of the function $g(\phi_{LO} - \phi_0)$ vs. ϕ_C for 3 different values of ζ . In general $0.5 \leq g_{\min} \leq 1$ for all values of ϕ_C and ζ , whereas, the lowest value $g_{\min} = 0.5$ is obtained in the limit $\zeta \rightarrow 1$. This limit corresponds to the case of operating close to a jump point, namely close to the edge of the bistability region.

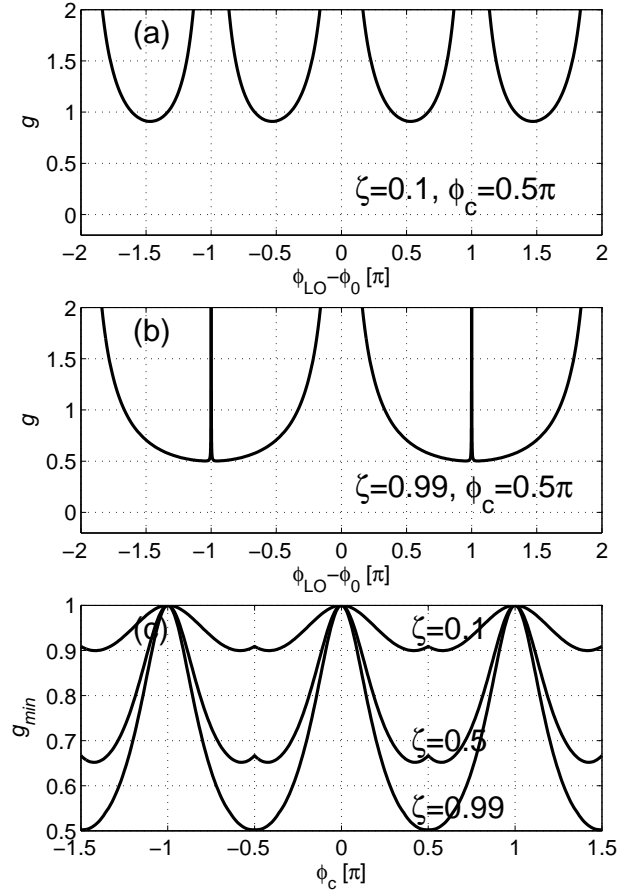


FIG. 3: The function g . Panel (a) shows $g(\phi_{LO} - \phi_0)$ for the case $\zeta = 0.1$ and $\phi_C = 0.5\pi$, and panel (b) for the case $\zeta = 0.99$ and $\phi_C = 0.5\pi$. Panel (c) shows the minimum value of the function $g(\phi_{LO} - \phi_0)$ vs. ϕ_C for different values of ζ .

X. CONCLUSIONS

In the present paper we analyze the performances of a nanomechanical mass detector. Both Kerr nonlinearity and nonlinear damping are taken into account to lowest order. The lower bound imposed upon the minimum detectable mass due to thermomechanical noise is generalized for the present case. The lowest detectable mass is obtained when the resonator is driven close to a jump point near the edge of the bistability region. However, in the same region slowing-down occurs in the response of the detector to a change in the mass (see Eq. (48)), limiting thus the detection speed. In general, for a given application the operating point can be chosen to optimally balance between the different requirements on the sensitivity and response time.

APPENDIX A: PRINCIPAL AXES

Consider an expansion of the function Θ near a complex number Z

$$\Theta(Z + z, Z^* + z^*) = \Theta_0 + Wz + Vz^* + O(|z|^2), \quad (\text{A1})$$

where $\Theta_0 = \Theta_0(Z, Z^*)$, and W and V are given by Eqs. (27) and (28) respectively.

The transformation

$$\begin{pmatrix} \xi \\ \eta \end{pmatrix} = \frac{1}{2} \begin{pmatrix} e^{i\phi} & e^{-i\phi} \\ -ie^{i\phi} & ie^{-i\phi} \end{pmatrix} \begin{pmatrix} z \\ z^* \end{pmatrix}, \quad (\text{A2})$$

represents axes rotation with angle ϕ (ϕ is real). The inverse transformation is given by

$$\begin{pmatrix} z \\ z^* \end{pmatrix} = \begin{pmatrix} e^{-i\phi} & ie^{-i\phi} \\ e^{i\phi} & -ie^{i\phi} \end{pmatrix} \begin{pmatrix} \xi \\ \eta \end{pmatrix}. \quad (\text{A3})$$

Using this notation one finds

$$Wz + Vz^* = R_\xi \xi + R_\eta \eta, \quad (\text{A4})$$

where

$$R_\xi = We^{-i\phi} + Ve^{i\phi}, \quad (\text{A5})$$

$$R_\eta = i(We^{-i\phi} - Ve^{i\phi}). \quad (\text{A6})$$

Principle axes are obtained by choosing $\phi = \phi_0$ where

$$e^{2i\phi_0} = \frac{WV^*}{|WV|}. \quad (\text{A7})$$

Thus, using the notation

$$\left(\frac{WV}{|WV|}\right)^{1/2} = e^{i\phi_a}, \quad (\text{A8})$$

one finds that in the reference frame of the principle axes the following hold

$$R_\xi = e^{i\phi_a}(|W| + |V|), \quad (\text{A9})$$

$$R_\eta = ie^{i\phi_a}(|W| - |V|), \quad (\text{A10})$$

and

$$Wz + Vz^* = e^{i\phi_a}[(|W| + |V|)\xi + i(|W| - |V|)\eta]. \quad (\text{A11})$$

ACKNOWLEDGMENT

This work is supported by the Israeli ministry of science, Intel Corp., Israel-US binational science foundation, and by Henry Gutwirth foundation.

-
- [1] E. A. Wachter and T. Thundat, *Rev. Sci. Instrum.* **66**, 3662 (1995).
 - [2] H. P. Lang, , R. Berger, , C. Andreoli, , J. Brugger, M. Despont, P. Vettiger, C. Gerber, et al., *Appl. Phys. Lett.* **72**, 383 (1998).
 - [3] Z. Y. Hu, T. Thundat, and R. J. Warmack, *J. Appl. Phys.* **90**, 427 (2001).
 - [4] B. Ilic, D. Czaplewski, H. G. Craighead, P. Neuzil, C. Campagnolo, and C. Batt, *Appl. Phys. Lett.* **77**, 450 (2000).
 - [5] J. Fritz, M. K. Baller, H. P. Lang, H. Rothuizen, P. Vettiger, E. Meyer, H. J. Guntherodt, C. Gerber, and J. K. Gimzewski, *Science* **288**, 316 (2000).
 - [6] B. Ilic, D. Czaplewski, M. Zalalutdinov, H. G. Craighead, P. Neuzil, C. Campagnolo, and C. Batt, *J. Vac. Sci. Technol. B* **19**, 2825 (2001).
 - [7] A. Subramanian, P. I. Oden, S. J. Kennel, K. B. Jacobson, R. J. Warmack, T. Thundat, and M. J. Doktycz, *Appl. Phys. Lett.* **81**, 385 (2002).
 - [8] B. Ilic, L. Yang, and H. G. Craighead, *Appl. Phys. Lett.* **85**, 2604 (2004).
 - [9] B. Ilic, H. G. Craighead, S. Krylov, W. Senarante, C. Ober, , and P. Neuzil, *J. Appl. Phys.* **95**, 3694 (2004).
 - [10] B. Ilic, Y. Yang, K. Aubin, R. Reichenbach, S. Krylov, and H. G. Craighead, *Nano Lett.* **5**, 925 (2005).
 - [11] K. L. Ekinci, X. M. H. H, and M. L. Roukes, *Appl. Phys. Lett.* **84**, 4469 (2004).
 - [12] M. K. Ghatkesar, V. Barwich, T. Braun, A. H. Bredekamp, U. Drechsler, M. Despont, H. P. Lang, M. Hegner, and C. Gerber, *Proc. IEEE Sensors* **2004**, 1060 (2004).
 - [13] S. Ghatnekar-Nilsson, E. Forsen, G. Abadal, J. Verd, F. Campabadal, F. Perez-Murano, J. Esteve, N. Barniol, A. Boisen, and L. Montelius, *Nanotechnology* **16**, 98 (2005).
 - [14] K. L. Ekinci, Y. T. Yang, and M. L. Roukes, *J. Appl. Phys.* **95**, 2682 (2004).
 - [15] A. N. Cleland, *New J. Phys.* **7**, 235 (2005).
 - [16] E. Wang and U. Heinz, *Phys. Rev. D* **66**, 025008 (2002).
 - [17] L. Landau and E. Lifshits, *Mechanics* (Oxford, New York, 1976).
 - [18] B. Yurke and E. Buks, *arXiv:quant-ph/0505018 v1* pp. 1–9 (2005).
 - [19] K. Wiesenfeld and B. McNamara, *Phys. Rev. A* **33**, 629 (1986).
 - [20] M. Dykman, D. Luchinsky, R. Mannella, P. McClintock,

- N. Stein, and N. Stocks, Phys. Rev. E **49**, 1198 (1994).
- [21] H. Kromer, A. Erbe, A. Tilke, S. Manus, and R. Blick, Europhys. Lett. **50**, 101 (2000).
- [22] S. Savel'ev, A. L. Rakhmanov, and F. Nori, Phys. Rev. E **72**, 056136 (2005).
- [23] H. B. Chan and C. Stambaugh, arXiv:cond-mat/0603037 (2006).
- [24] R. Almog, S. Zaitsev, O. Shtempluck, and E. Buks, Appl. Phys. Lett. **88**, 213509 (2006).
- [25] R. Almog, S. Zaitsev, O. Shtempluck, and E. Buks, arXiv: cond-mat/0607055 (2006).
- [26] D. Rugar and P. Grutter, Phys. Rev. Lett. **67**, 699 (1991).
- [27] S. Zaitsev and E. Buks, arXiv: cond-mat/0503130 (2005).
- [28] C. W. Gardiner and M. J. Collett, Phys. Rev. A **31**, 3761 (1985).
- [29] E. Buks and B. Yurke, Phys. Rev. A **73**, 023815 (2006).